EDGE ARTICLE

Check for updates

Polymorph exploration of bismuth stannate using first-principles phonon mode mapping†

Warda Rahim, [ID] [ab] Jonathan M. Skelton,[c] Christopher N. Savory, [ID] [ab] Ivana R. Evans, [ID] [d] John S. O. Evans,[d] Aron Walsh [ID] [ef] and David O. Scanlon [ID] *[abg]

Accurately modelling polymorphism in crystalline solids remains a key challenge in computational chemistry. In this work, we apply a theoretically-rigorous phonon mode-mapping approach to understand the polymorphism in the ternary metal oxide $Bi_2Sn_2O_7$. Starting from the high-temperature cubic pyrochlore aristotype, we systematically explore the structural potential-energy surface and recover the two known low-temperature phases alongside three new metastable phases, together with the transition pathways connecting them. This first-principles lattice-dynamics method is completely general and provides a practical means to identify and characterise the stable polymorphs and phase transitions in materials with complex crystal structures.

1 Introduction

Predicting polymorphism using first-principles methods is a fundamental challenge in materials discovery.[1–3] The ability to search for and identify polymorphs computationally both helps avoid experimental complications from poor-quality samples and low-resolution characterisation, and also accelerates the development of functional materials.

Group-theoretical methods have successfully been used to characterise the lower-symmetry phases derived by distorting the archetypal cubic ABX_3/$A_2BB'X_6$ perovskite phase by tilting and distorting the BX_6/$B'X_6$ octahedra.[4–8] Predicting polymorphs in complex multi-component systems presents a major challenge, as the number of degrees of freedom often makes *ab initio* exploration prohibitively expensive.

In this study, we remap the problem of identifying polymorphs of the ternary metal oxide $Bi_2Sn_2O_7$ from a search over atom positions in real space to collective atomic displacements in phonon space.[9] This results in an efficient and unbiased computational approach to predicting the polymorphs of the ternary oxide $Bi_2Sn_2O_7$, which is generally applicable to other complex systems where conventional approaches such as random searching or genetic algorithms are not practical.[10–14]

1.1 Crystal chemistry of bismuth stannate

The ideal $A_2B_2O_6O'$ pyrochlore structure in the $Fd\bar{3}m$ space group has eight formula units in the unit cell. The four unique atomic sites, *viz.* the A-site cation (+2 or +3), B-site cation (+4 or +5), and two inequivalent oxygen sites (O and O'), are present at the 16c, 16d, 48f and 8a Wyckoff positions, respectively.[15] The inequivalent O sites can be understood as two interpenetrating oxide sublattices.[16] The B-site cation forms corner-sharing BO_6 octahedra, while the A-site cation adopts an anti-cristobalite geometry based on corner-sharing A_4O' tetrahedra with linear O'–A–O' bonds. The interpenetration of the oxide sublattices results in distorted hexagonal bipyramidal coordination at the

[a]Department of Chemistry, University College London, 20 Gordon Street, London WC1H 0AJ, UK. E-mail: d.scanlon@ucl.ac.uk

[b]Thomas Young Centre, University College London, Gower Street, London WC1E 6BT, UK

[c]Department of Chemistry, University of Manchester, Oxford Road, Manchester M13 9PL, UK

[d]Department of Chemistry, University Science Site, Durham University, South Road, Durham DH1 3LE, UK

[e]Department of Materials, Imperial College London, Exhibition Road, London SW7 2AZ, UK

[f]Department of Materials Science and Engineering, Yonsei University, Seoul 03722, Korea

[g]Diamond Light Source Ltd., Diamond House, Harwell Science and Innovation Campus, Didcot, Oxfordshire OX11 0DE, UK

† Electronic supplementary information (ESI) available. See DOI: 10.1039/d0sc02995e
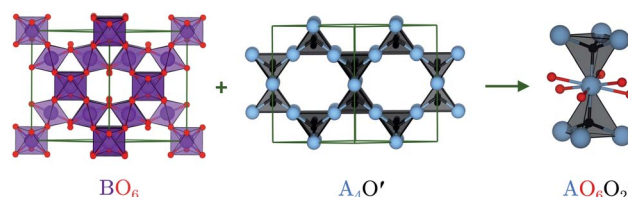
Fig. 1 Pyrochlore structure showing the two oxide sublattices forming a corner-sharing network of BO_6 octahedra and an anti-cristobalite network of corner-sharing A_4O' tetrahedra. Interpenetration of the two networks results in a bipyramidal hexagonal A-site coordination environment with 6 equatorial O and two axial O'. The atoms are coloured as follows: A-site – blue, B-site – purple, O – red, and O' – black. The images were generated using VESTA.[17]

A-site, with six longer equatorial A–O bonds and two shorter axial A–O′ bonds (Fig. 1).

Bi$_2$Sn$_2$O$_7$ is unique in undergoing symmetry-lowering phase transitions on cooling and has three well-characterised polymorphs: the high-temperature cubic γ phase undergoes a second-order phase transition to β-Bi$_2$Sn$_2$O$_7$ above 900 K, followed by a first-order phase transition to α-Bi$_2$Sn$_2$O$_7$ around 390 K.[18] γ-Bi$_2$Sn$_2$O$_7$ possesses the standard cubic pyrochlore structure with the Bi^{3+} cations displaced from the ideal crystallographic sites.[19] While the structure of γ-Bi$_2$Sn$_2$O$_7$ is undisputed, characterising the structures of β- and α-Bi$_2$Sn$_2$O$_7$ has been a significant challenge.

The first structural model for α-Bi$_2$Sn$_2$O$_7$ was a non-centrosymmetric monoclinic $P1c1$ structure with 352 atoms per cell[20] (α$_{old}$). Three assumptions were used to solve the structure: (1) that β-Bi$_2$Sn$_2$O$_7$ has a face-centred cubic structure, (2) that β- and α-Bi$_2$Sn$_2$O$_7$ are second-harmonic generation active; and (3) that the three phases have group–subgroup relations.[18]

New insight was obtained very recently from high-resolution X-ray and neutron powder diffraction.[16] Though the neutron data showed β to be metrically cubic, small peak splittings in the X-ray data indicated a lower-symmetry structure. An exhaustive symmetry-adapted distortion mode approach was used to enumerate all the candidate structures between the high-symmetry γ parent and a base $P1$ child structure using ISODISTORT.[21,22] All the candidate structures were then tested against room-temperature and ~470 K X-ray and neutron data, based on which an orthorhombic $Aba2$ structure with 176 atoms in the conventional cell was suggested for β-Bi$_2$Sn$_2$O$_7$ together with a simplified Cc structure with 88 atoms per cell for α-Bi$_2$Sn$_2$O$_7$ (α$_{new}$). The four structures, $viz.$ γ, β, α$_{old}$ and α$_{new}$, are shown in Fig. 2.

2   Results and discussion

2.1   Phonon mode mapping procedure

Starting from the high-temperature γ structure, we employ an ab $initio$ approach to systematically identify the energy minima on the structural potential-energy surface (PES) of Bi$_2$Sn$_2$O$_7$.

The harmonic phonon dispersion of γ-Bi$_2$Sn$_2$O$_7$ is evaluated using the supercell finite-displacement method[23,24] with the Phonopy package.[25] Imaginary harmonic modes in the dispersion indicate dynamical instabilities in the form of collective atomic displacements that lower the energy. We use the ModeMap code[26] to map the energy as a function of the normal-mode coordinate Q (distortion amplitude) along the imaginary-mode eigenvectors and to locate the energy minimum along the mode. This structure is then relaxed and a subsequent phonon calculation performed to check for additional imaginary modes. Repeating this procedure iteratively across all the imaginary modes in the parent γ and child structure(s) until each branch terminates in a dynamically-stable structure with no imaginary modes allows the sequence of intermediate structures connecting the γ and low-temperature α-phases to be systematically enumerated while also identifying other (meta-)stable polymorphs.

We use plane-wave density-functional theory with the PBEsol functional for the force calculations, as PBEsol has been shown to give accurate structures and phonon frequencies.[26–30] Full details of the computational modelling and mode-mapping procedure are given in the ESI.†

2.2   Distorting the cubic aristotype

The phonon dispersion of γ-Bi$_2$Sn$_2$O$_7$ shows imaginary modes at four phonon wavevectors, $viz.$ a triply-degenerate mode at Γ, doubly-degenerate modes at W and X, and single- and a doubly-degenerate modes at L (Fig. 3). The wavevector defines the periodicity of the distortion, and the $q_\Gamma = (0, 0, 0)$ wavevector is commensurate with the unit cell and the distortions therefore do not change the cell volume. We therefore began our exploration by mapping the three Γ-point modes to obtain the typical double-well potential-energy curves shown in Fig. 3. The three imaginary modes lead to minima 3.17–3.35 meV per atom lower in energy than γ-Bi$_2$Sn$_2$O$_7$.

After relaxation we obtain an orthorhombic $Ima2$ structure with 44 atoms per cell. The dispersion of this structure has imaginary modes at four wavevectors, $viz.$ Γ, R, X and T. Mapping the Γ-point instability leads to a 44-atom monoclinic
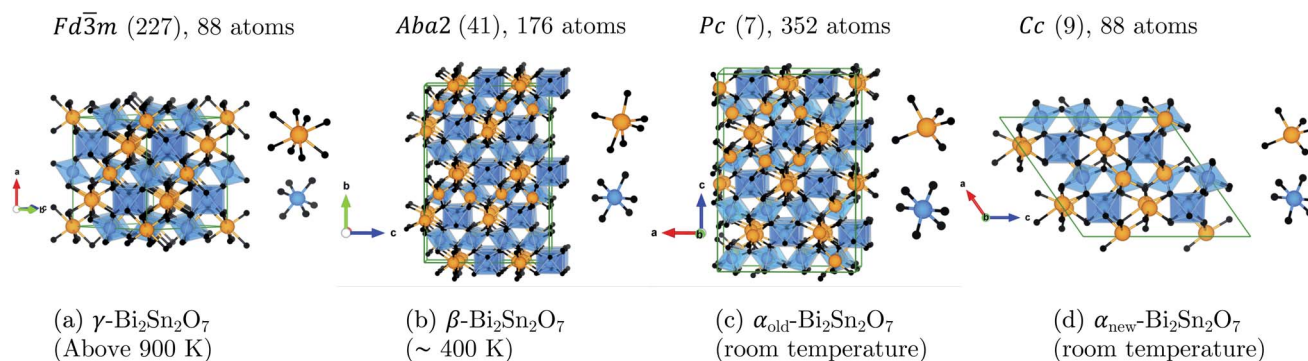

$Fd\bar{3}m$ (227), 88 atoms $Aba2$ (41), 176 atoms Pc (7), 352 atoms Cc (9), 88 atoms

(a) γ-Bi$_2$Sn$_2$O$_7$ (Above 900 K)   (b) β-Bi$_2$Sn$_2$O$_7$ (~ 400 K)   (c) α$_{old}$-Bi$_2$Sn$_2$O$_7$ (room temperature)   (d) α$_{new}$-Bi$_2$Sn$_2$O$_7$ (room temperature)

Fig. 2   Unit cells of (a) the cubic pyrochlore γ-Bi$_2$Sn$_2$O$_7$ structure with statistically averaged Bi^{3+} displacements and the distorted (b) β, (c) α$_{old}$, and (d) α$_{new}$ structures. All four structures are aligned along the SnO$_6$ octahedra to show the increasingly-irregular Bi chains as the temperature decreases. The insets show the cation coordination in each structure. The atoms are coloured as follows: Bi – orange, Sn – blue, O and O′ – black. These images were generated using VESTA.[17]
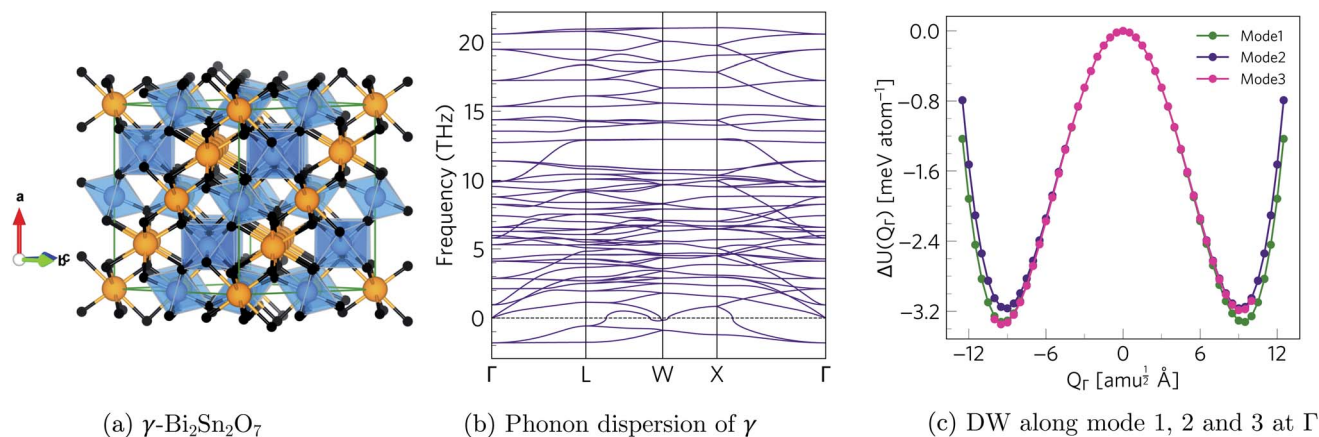
(a) γ-Bi$_2$Sn$_2$O$_7$ (b) Phonon dispersion of γ (c) DW along mode 1, 2 and 3 at Γ

Fig. 3 (a) Crystal structure of γ-Bi$_2$Sn$_2$O$_7$. (b) Phonon dispersion of γ-Bi$_2$Sn$_2$O$_7$ showing imaginary frequencies at the Γ, L, W and X phonon wavevectors. (c) Double-well (DW) potential-energy surface along the three Γ-point imaginary modes.

Cc structure with a single imaginary mode at $\mathbf{q}_V = \left(\frac{1}{2}, 0, 0\right)$ (Fig. S3 and S4†). For this mode, a complete distortion period requires a $2 \times 1 \times 1$ supercell, and mapping yields the 88-atom Cc α_{new} structure.[16] (Calculated: $a = 13.108$ Å, $b = 7.559$ Å, $c = 13.115$ Å and $\beta = 109.6°$; measured:[16] $a = 13.155$ Å, $b = 7.541$ Å, $c = 13.146$ Å and $\beta = 110.04°$.) Our method therefore yields the room-temperature α_{new} polymorph from the high-temperature γ phase in three mode-mapping steps. The phonon dispersion of α_{new} has no imaginary modes, indicating it to be a dynamically-stable energy minimum.

Since each of the instabilities in γ-Bi$_2$Sn$_2$O$_7$ represents different possible transition pathways, we mapped all the independent imaginary modes to try and locate the β phase or other stable polymorphs. The instabilities at X and W were mapped in $2 \times 1 \times 2$ and $2 \times 4 \times 4$ supercells, respectively, commensurate with the $\mathbf{q}_X = \left(\frac{1}{2}, 0, \frac{1}{2}\right)$ and $\mathbf{q}_W = \left(\frac{1}{2}, \frac{1}{4}, \frac{3}{4}\right)$ wavevectors (Fig. 4). The instability at X leads in a single step to a dynamically-stable $P2_12_12_1$ structure with 44 atoms per cell via a double-well with a depth of ~0.714 meV per atom. The W-point instability leads to a dynamically-stable $Pna2_1$ structure
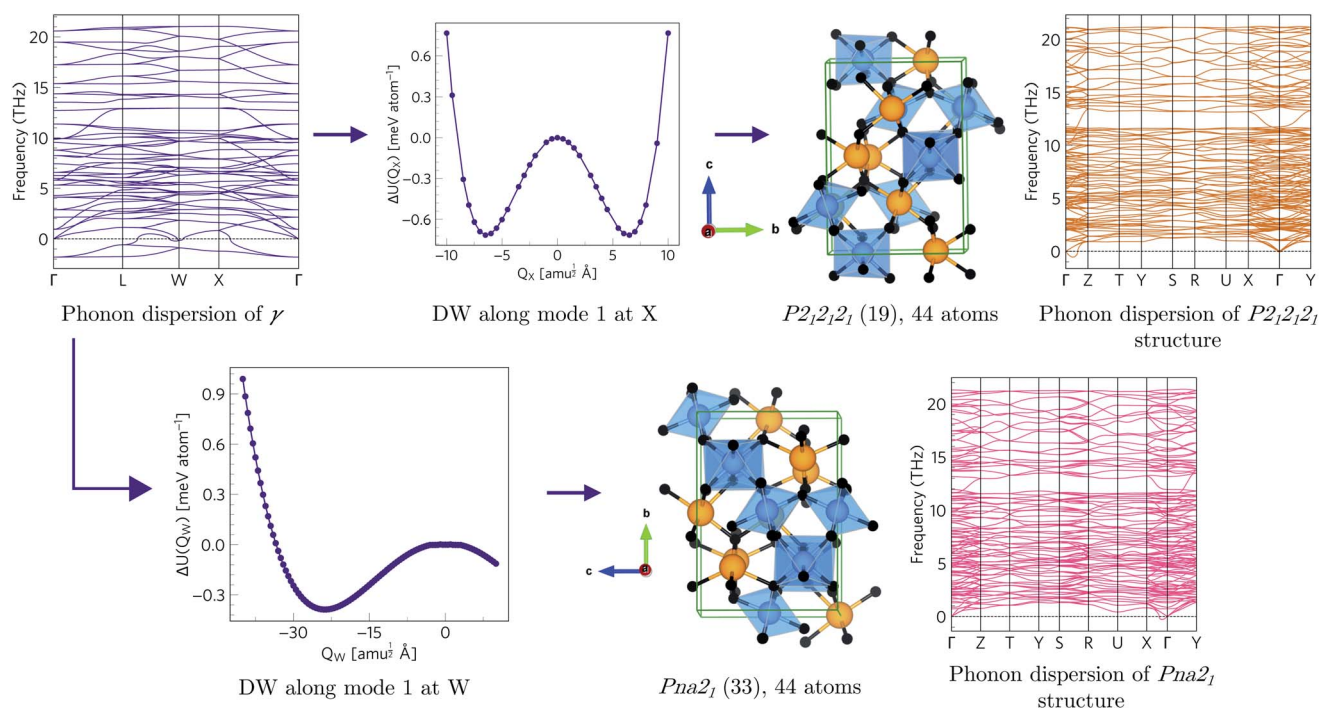

Phonon dispersion of γ DW along mode 1 at X $P2_12_12_1$ (19), 44 atoms   Phonon dispersion of $P2_12_12_1$ structure

DW along mode 1 at W $Pna2_1$ (33), 44 atoms   Phonon dispersion of $Pna2_1$ structure

Fig. 4 Transition pathways starting from the X- and W-point instabilities in the γ-Bi$_2$Sn$_2$O$_7$ dispersion (top left). The X-point instability leads to a $P2_12_12_1$ structure (top row) while the W-point mode leads to a $Pna2_1$ structure (bottom row). Both structures are dynamically stable with no imaginary modes in the dispersions. (The imaginary acoustic mode along the $\Gamma \rightarrow$ Z path in the $P2_12_12_1$ is an interpolation artefact – see ESI.†)
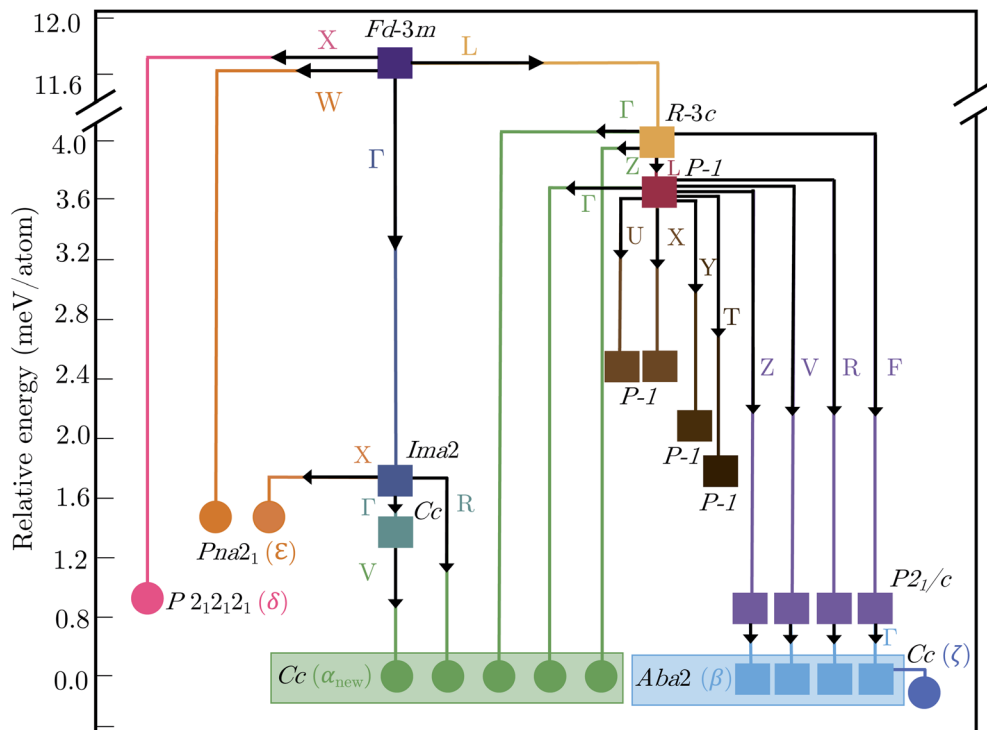
Fig. 5 Tree diagram showing the polymorphism in $Bi_2Sn_2O_7$ starting from the high-temperature γ polymorph (purple square). Energies are shown relative to the α_{new}-phase (green circle). Branches trace the transition pathways obtained by distorting along single imaginary harmonic modes at each step. Circles and squares indicate dynamically stable and unstable structures, respectively, with the space groups as marked. The wavevectors of the imaginary modes connecting pairs of structures are indicated next to the solid lines.

via a double-well potential with a depth of ~0.388 meV per atom, again with 44 atoms per cell. Neither polymorph has yet been identified experimentally, and we refer to the $P2_12_12_1$ and $Pna2_1$ structures as δ-$Bi_2Sn_2O_7$ and ε-$Bi_2Sn_2O_7$ respectively. The δ and ε phases are 0.87 and 1.45 meV per atom higher in energy than α_{new} and are thus metastable.

Finally, mapping the L-point instability in γ-$Bi_2Sn_2O_7$ in a 2 × 2 × 2 supercell also leads to the α_{new} structure in two steps *via* an intermediate $R\bar{3}c$ (167) phase with 132 atoms per unit cell (Fig. S6†).

We next proceeded to analyse the other instabilities present in the intermediate structures (Fig. S7–S10†). Several pathways end in α_{new}, while several others lead to the intermediate-temperature β phase.[16] More pathways lead to α_{new}, suggesting it may be more accessible on the PES.

The dispersion of β-$Bi_2Sn_2O_7$ has imaginary modes at the Γ and Y wavevectors. Both double-well potentials have a very shallow depth of ~7×10^{-3} meV per atom and lead to a stable Cc structure with 176 atoms per cell (ζ-$Bi_2Sn_2O_7$; Fig. S11†). This indicates that the β phase is likely a thermal average of equivalent lower-symmetry ζ structures.

To investigate this, we performed Rietveld analysis of a series of powder diffraction patterns collected from 300–1100 K in which the isotropic atomic displacement parameters (ADPs) of the inequivalent Bi sites were independently refined (4 in α, 5 in β, 1 in γ). The ADPs can provide valuable structural information,[31–33] and while this analysis pushes the information content of powder

diffraction to its limits, we find that the Bi4 and Bi5 atoms, which disorder during the phase transition, have ADPs in the β phase comparable to those in γ-$Bi_2Sn_2O_7$ and much larger than the other Bi atoms (Fig. S12†). Similarly, the calculated ADPs for β-$Bi_2Sn_2O_7$ predict large-amplitude displacements of these atoms.

We further tested the model against the data in ref. 16 with a Rietveld methodology such that the R-factors are directly comparable. Splitting the Bi4 site produces an excellent fit to the neutron and X-ray powder diffraction data and reduces R_{wp} from 4.355% without splitting to 4.176%. This is also lower than the 4.201% obtained by reducing the symmetry to monoclinic. This provides further evidence that the site is dynamically disordered, as predicted by our calculations, and indicates that ζ-$Bi_2Sn_2O_7$ represents the true local structure of the intermediate-temperature phase.

2.3 Polymorph map

Fig. 5 shows the complete polymorph map for $Bi_2Sn_2O_7$ as a tree diagram. Each branch connects intermediate structures linked by continuous atomic displacements and terminates at structures with no dynamical instabilities. The energies decrease along all pathways with no energetic barriers. Apart from the two new metastable δ and ε phases, all other branches lead to α- and β-/ζ-$Bi_2Sn_2O_7$. A series of intermediate $P\bar{1}$ structures with dynamical instabilities were also identified, but the instabilities were not mapped. From their position on the diagram, however, we can infer that they would likely lead to α- or β-$Bi_2Sn_2O_7$.

The small energy separations between minima highlight the complexity of the PES and indicate that different synthesis conditions may yield different polymorphs by changing the free-energy landscape during crystal formation.[34] With the exception of β- and ζ-$Bi_2Sn_2O_7$, all the structures are higher in energy than α_{new}. However, these energies are the lattice energies from athermal electronic-structure calculations, and free-energy contributions from lattice vibrations and temperature effects are likely to change the energetic ordering. β- and ζ-$Bi_2Sn_2O_7$ are predicted to be only 0.1 and 0.19 meV per atom lower in energy than the α phase, respectively, and taken together with the experimental data this suggests that α_{new} is the global energy minimum on the PES.

Future work may employ the quasi-harmonic approximation (QHA) to compute the temperature-dependent Gibbs free energy G and obtain a more accurate free-energy landscape, improved relative stabilities, and predicted phase-transition temperatures.[35]

2.4 Chemical explanation of distortions

The structural distortions underlying the polymorphism in $Bi_2Sn_2O_7$ are driven by the stereochemically-active Bi 6s lone pair. Interaction of the Bi 6s and O 2p states produces filled antibonding orbitals at the top of the valence band, which facilitate coupling to the metal 6p states.[36] This hybridisation is symmetry forbidden in the cubic γ phase, but instantaneous symmetry breaking from vibrations allows the Bi 6p and Bi 6s/O 2p states to couple. This stabilises the filled antibonding orbital and offsets the increase in energy from the structural distortion, thereby favouring lower-symmetry structures.[37–40]

This model is supported from the symmetry-mode analysis of the diffraction data by the larger amplitudes of distortion modes associated with Bi_4O' tetrahedra compared to those of SnO_6 octahedra.[16] This is also consistent with the eigenvectors of the imaginary modes involved in the γ → α_{new} transition path (Fig. S13†), which show coupled rotations of the Bi and O' atoms with very little movement of Sn.

3 Conclusions

We have employed a first-principles lattice-dynamics approach to systematically explore the structural PES of $Bi_2Sn_2O_7$ starting from the high-temperature cubic pyrochlore aristotype. We recover the known phases from diffraction measurements and identify three new dynamically-stable polymorphs that may be targets for future experimental syntheses. We further demonstrate that the intermediate-temperature β polymorph is a crystallographic average over a lower-symmetry ζ minimum, the structure of which is supported by the diffraction data.

$Bi_2Sn_2O_7$ is the most complex system yet to be solved using a computational approach, highlighting the strength of our mode-mapping technique for complex multiternary structures, and this approach could be readily extended to other materials with high-symmetry parent structures such as leucite/pollucite,[41] moganite[42] and andorite.[43]

Notes and references

1 J. Maddox, *Nature*, 1988, **201**, 335.
2 A. van de Walle, *Nat. Mater.*, 2005, **4**, 362.
3 N. L. Abraham and M. I. J. Probert, *Phys. Rev. B: Condens. Matter Mater. Phys.*, 2006, **73**, 224104.
4 C. J. Howard and H. T. Stokes, *Acta Crystallogr., Sect. B: Struct. Sci.*, 1998, **54**, 782.
5 H. T. Stokes, E. H. Kisi, D. M. Hatch and C. J. Howard, *Acta Crystallogr., Sect. B: Struct. Sci.*, 2002, **58**, 934.
6 C. J. Howard and M. A. Carpenter, *Acta Crystallogr., Sect. B: Struct. Sci.*, 2010, **66**, 40.
7 B. Orayech, I. Urcelay-Olabarria, G. A. López, O. Fabelo, A. Faik and J. M. Igartua, *Dalton Trans.*, 2015, **44**, 13867.
8 J. Young, A. Stroppa, S. Picozzi and J. M. Rondinelli, *Dalton Trans.*, 2015, **44**, 10644.
9 A. Togo and I. Tanaka, *Phys. Rev. B: Condens. Matter Mater. Phys.*, 2013, **87**, 184104.
10 C. J. Pickard and R. J. Needs, *J. Phys.: Condens. Matter*, 2011, **23**, 053201.
11 A. E. Eiben and J. E. Smith, in *Introd. to Evol. Comput.*, Springer, Berlin, Heidelberg, 2015, p. 25.
12 N. L. Abraham and M. I. J. Probert, *Phys. Rev. B: Condens. Matter Mater. Phys.*, 2006, **73**, 224104.
13 S. Q. Wu, M. Ji, C.-Z. Wang, M. C. Nguyen, X. Zhao, K. Umemoto, R. M. Wentzcovitch and K.-M. Ho, *J. Phys.: Condens. Matter*, 2013, **26**, 035402.
14 S. Y. Chen, F. Zheng, S. Q. Wu and Z. Z. Zhu, *Curr. Appl. Phys.*, 2017, **17**, 454.
15 B. J. Kennedy, B. A. Hunter and C. J. Howard, *J. Solid State Chem.*, 1997, **130**, 58.
16 J. W. Lewis, J. L. Payne, I. R. Evans, H. T. Stokes, B. J. Campbell and J. S. O. Evans, *J. Am. Chem. Soc.*, 2016, **138**, 8031.
17 K. Momma and F. Izumi, *J. Appl. Crystallogr.*, 2011, **44**, 1272.
18 R. D. Shannon, J. D. Berlein, J. L. Gillson, G. A. Jon and A. W. Sleight, *J. Phys. Chem. Solids*, 1980, **41**, 117.
19 V. Kahlenberg, *Z. Kristallogr.*, 1997, **212**, 297.
20 I. R. Evans, J. A. K. Howard and J. S. O. Evans, *J. Mater. Chem.*, 2003, **13**, 2098.
21 B. J. Campbell, H. T. Stokes, D. E. Tanner and D. M. Hatch, *J. Appl. Crystallogr.*, 2006, **39**, 607.

22 H. T. Stokes, D. M. Hatch and B. J. Campbell, *ISOTROPY Software Suite*, 2017, http://stokes.byu.edu/isotropy.html.

23 K. Parlinski, Z. Q. Li and Y. Kawazoe, *Phys. Rev. Lett.*, 1997, **78**, 4063.

24 G. Kresse, J. Furthmüller and J. Hafner, *Europhys. Lett.*, 1995, **32**, 729.

25 A. Togo and I. Tanaka, *Scr. Mater.*, 2015, **108**, 1.

26 J. M. Skelton, L. A. Burton, S. C. Parker, A. Walsh, C.-E. Kim, A. Soon, J. Buckeridge, A. A. Sokol, C. R. A. Catlow, A. Togo and I. Tanaka, *Phys. Rev. Lett.*, 2016, **117**, 075502.

27 J. M. Skelton, D. Tiana, S. C. Parker, A. Togo, I. Tanaka and A. Walsh, *J. Chem. Phys.*, 2015, **143**, 64710.

28 A. M. Ganose, K. T. Butler, A. Walsh and D. O. Scanlon, *J. Mater. Chem. A*, 2016, **4**, 2060.

29 M. A. Tumelero, L. C. Benetti, E. Isoppo, R. Faccio, G. Zangari and A. A. Pasa, *J. Phys. Chem. C*, 2016, **120**, 11797.

30 C. N. Savory, A. M. Ganose and D. O. Scanlon, *Chem. Mater.*, 2017, **29**, 5156.

31 A. E. Phillips, G. J. Halder, K. W. Chapman, A. L. Goodwin and C. J. Kepert, *J. Am. Chem. Soc.*, 2010, **132**, 10.

32 E. E. McCabe, D. G. Free, B. G. Mendis, J. S. Higgins and J. S. O. Evans, *Chem. Mater.*, 2010, **22**, 6171.

33 S. Lee and H. Xu, *Acta Crystallogr., Sect. B: Struct. Sci., Cryst. Eng. Mater.*, 2019, **75**, 160.

34 W. Sun, S. T. Dacek, S. P. Ong, G. Hautier, A. Jain, W. D. Richards, A. C. Gamst, K. A. Persson and G. Ceder, *Sci. Adv.*, 2016, **2**, e1600225.

35 E. Lora Da Silva, J. M. Skelton, S. C. Parker and A. Walsh, *Phys. Rev. B: Condens. Matter Mater. Phys.*, 2015, **91**, 144107.

36 A. Walsh, D. J. Payne, R. G. Egdell and G. W. Watson, *Chem. Soc. Rev.*, 2011, **40**, 4455.

37 A. Walsh and G. W. Watson, *Phys. Rev. B: Condens. Matter Mater. Phys.*, 2004, **70**, 235114.

38 A. Walsh and G. W. Watson, *J. Solid State Chem.*, 2005, **178**, 1422.

39 A. Walsh, G. W. Watson, D. J. Payne, G. Atkinson and R. G. Egdell, *J. Mater. Chem.*, 2006, **16**, 3452.

40 A. Walsh and G. W. Watson, *Chem. Mater.*, 2007, **19**, 5158.

41 K. S. Knight and C. M. B. Henderson, *Phys. Chem. Miner.*, 2019, **46**, 595.

42 J. Haines, C. Chateau, J. M. Léger, A. Le Sauze, N. Diot, R. Marchand and S. Hull, *Acta Crystallogr., Sect. B: Struct. Sci.*, 1999, **55**, 677.

43 M. Nespolo, T. Ozawa, Y. Kawasaki and K. Sugiyama, *J. Mineral. Petrol. Sci.*, 2012, **107**, 226.